

Methanol as a carrier of hydrogen and carbon in fossil-free production of direct reduced iron

Joakim Andersson^{a,*}, Andries Krüger^b, Stefan Grönkvist^a

^a Division of Energy Processes, KTH Royal Institute of Technology, SE-10044 Stockholm, Sweden

^b Division of Applied Electrochemistry, KTH Royal Institute of Technology, SE-10044 Stockholm, Sweden

ARTICLE INFO

Keywords:

Direct reduced iron
Fossil-free steelmaking
Methanol
Electrolysis
Hydrogen storage
Industrial decarbonization

ABSTRACT

Steelmaking is responsible for around 7% of the global emissions of carbon dioxide and new steelmaking processes are necessary to reach international climate targets. As a response to this, steelmaking processes based on the direct reduction of iron ore by hydrogen produced via water electrolysis powered by renewable electricity have been suggested. Here we present a novel variant of hydrogen-based steelmaking incorporating methanol as a hydrogen and carbon carrier together with high-temperature co-electrolysis of water and carbon dioxide and biomass oxy-fuel combustion. The energy and mass balances of the process are analyzed. It is found that this methanol-based direct reduction process may potentially offer a number of process-related advantages over a process based on pure hydrogen, featuring several process integration options. Notably, the electricity and total energy use of the steelmaking process could be reduced by up to 25% and 8% compared to a reference pure-hydrogen process, respectively. The amount of high-temperature (> 200 °C) heat that must be supplied to the process could also be reduced by up to approximately 34%, although the demand for medium-temperature heat is substantially increased. Furthermore, the suggested process could allow for the production of high-quality direct reduced iron with appropriate carburization to alleviate downstream processing in an electric arc furnace, which is not the case for a process based on pure hydrogen.

1. Introduction

Iron ore-based steelmaking is currently responsible for around 7% of global carbon dioxide (CO_2) emissions [1]. Reducing these emissions to meet climate targets is challenging as the currently dominating form of steelmaking, the blast furnace-basic oxygen furnace (BF-BOF) process, is dependent on coal as a reductant and fuel [2–4]. In essence, there are two options for reducing CO_2 emissions from steelmaking: to keep the BF-BOF process and implement carbon capture and storage (CCS) technology, or to seek new low-emissions processes [5]. One of the alternative processes currently considered promising is the production of direct reduced iron (DRI) via hydrogen (H_2) direct reduction (H-DR) [6]. Produced DRI may be refined to steel using an electric arc furnace (EAF) [7]. H-DR steelmaking is the basis of the HYBRIT (HYdrogen BReakthrough Ironmaking Technology) initiative, a collaboration between SSAB (steelmaking), Luossavaara-Kiirunavaara Aktiebolag (LKAB) (mining), and Vattenfall (energy utility). The goal of the HYBRIT project is to achieve full-scale implementation of H-DR by 2035 [1].

The H-DR process replaces the conventional coal-based reductant of

the BF-BOF process with H_2 produced via the electrolysis of water (H_2O). As electrolysis is an inherently electricity-intensive process, the large-scale implementation of H-DR is expected to affect the Swedish energy system significantly; replacing all current BF capacity in Sweden with H-DR could increase electricity consumption by as much as 10% of the current total Swedish electricity production [8].

A key part of managing the large electricity demand of the H-DR process is the incorporation of an H_2 storage. An H_2 storage allows for the discontinuous production of H_2 while maintaining constant steel production. This decoupling of H_2 and steel production allows for the electrolyzer load to be lowered during times of high electricity prices and vice versa. In this way, the average H_2 cost is reduced – granted that the costs associated with the storage do not outweigh the reduced H_2 production costs. Furthermore, the flexibility afforded by an H_2 storage makes it possible for the electrolyzers to provide additional grid services.

There are very few large-scale storages of H_2 in operation, all being salt caverns [9]. These caverns are created by pumping water into an underground salt formation to dissolve part of the salt, after which the produced salt- H_2O mixture is pumped out, leaving a cavity suitable for

* Corresponding author.

E-mail addresses: joakim9@kth.se (J. Andersson), andriesk@kth.se (A. Krüger), stefangr@kth.se (S. Grönkvist).

Nomenclature

AEL	Alkaline electrolysis
ASU	Air separation unit
BF	Blast furnace
BOF	Basic oxygen furnace
CCS	Carbon capture and storage
c_p°	Specific heat capacity
DR	Direct reduction
DRI	Direct reduced iron
EAF	Electric arc furnace
H°	Specific standard enthalpy
H-DR	Hydrogen direct reduction
HHV	Higher heating value
HYBRIT	Hydrogen Breakthrough Ironmaking Technology
LHV	Lower heating value
M	Degree of metallisation

MAF	Moisture- and ash-free substance
MD	Methanol decomposition
MEA	Monoethanolamine
M_w	Molar weight
\dot{n}	Molar flow
NIST	National Institute of Standards and Technology
OSR	Oxidative steam reforming
PEMEL	Proton exchange membrane electrolysis
POX	Partial oxidation
PSA	Pressure swing adsorption
SOEL	Solid oxide electrolysis
SR	Steam reforming
T	Temperature
t	Temperature in Kelvin divided by 1 000
ΔH_R	Enthalpy of reaction
ΔH_{vap}	Enthalpy of vaporization

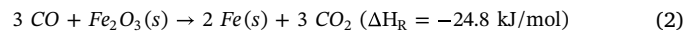
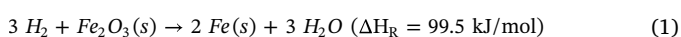
H₂ storage [10]. Unfortunately, salt cavern storages, along with other possibly promising options for the underground storage of large amounts of H₂, e.g., aquifers and depleted natural gas fields, require certain geological conditions [9]. In many regions of the world, including Sweden, these conditions cannot be met and, therefore, alternative solutions are required for large-scale H₂ storage [11].

H₂ can principally be stored via several other routes beyond as a compressed gas [12]. One such route is the reaction of H₂ with CO₂ to form methanol (CH₃OH) and H₂O. This CH₃OH-H₂O mixture can then be converted back to H₂ via a reforming process. By utilizing this CH₃OH-based system, H₂ can be stored at high density (99 kg H₂/m³ for pure CH₃OH or 107 kg H₂/m³ for a stoichiometric CH₃OH-H₂O mixture) in liquid form at ambient conditions.

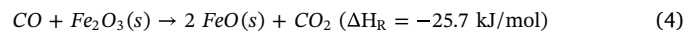
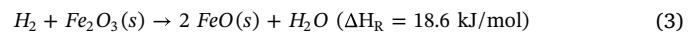
The remainder of this article aims to explore how an H₂ storage in the form of CH₃OH may be integrated into an H-DR process and what the possible advantages of such integration could be. In particular, the incorporation of a CH₃OH-based H₂ storage enables the possibility of utilizing the CO₂ formed in the carbon monoxide-based (CO) iron ore reduction and carburization reactions to store H₂. Further objectives of this article are to evaluate the effects that DRI carburization and reducing gas CO content have on the overall mass and energy balances of a DR process. Another objective is to evaluate possible advantages of the production of CO from CO₂ in an H-DR process, in particular via the high-temperature co-electrolysis of steam and CO₂. Furthermore, oxygen (O₂) co-produced with H₂ in electrolysis can be utilized for biomass oxy-fuel combustion to provide heat and carbon to the process. The starting point for the analysis is a review of the principles for the production of DRI in existing natural gas-based DR processes, the currently existing commercially applied steelmaking processes that closest resemble the H-DR process.

1.1. Conventional direct reduction processes

A distinguishing feature of DR processes is that the product of the reduction – the DRI – remains in solid phase, in contrast to the molten pig iron obtained from the BF. The most widely applied reactor design in DR processes is the reduction shaft, or shaft furnace, which is a solid-gas countercurrent moving bed reactor [13]. In the reduction shaft, iron ore pellets, consisting mainly of hematite (Fe₂O₃), flow downwards under the effect of gravity against a counter flow of reducing gas, a mixture of predominantly H₂ and CO most commonly produced via the reforming of natural gas (which mostly consists of methane (CH₄)) [14,15]. The reducing gas reacts with the Fe₂O₃ to form metallic iron (Fe) via the following overall reduction reactions [16]:

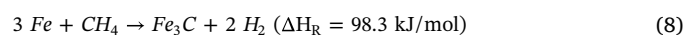
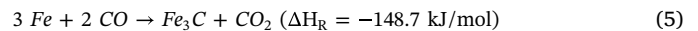


Two other iron oxides are formed as intermediates on the way towards Fe: first magnetite (Fe₃O₄), then wüstite (FeO) [17]. The DRI product is never fully reduced in conventional DR processes, i.e., some iron oxide remains in the product DRI in the form of FeO, formed via reactions (3) and (4) [18].



The share of the Fe in incoming Fe₂O₃ that is fully reduced is referred to as the DRI ‘metallisation’. DRI metallisation is generally in the range 90–96% (by mole) in conventional DR processes [19,20]. While theoretically advantageous, higher degrees of metallisation are not viable due to the kinetics of the commercial processes [14,20–22].

Conventional DRI typically contains some amount of carbon, originating from CO or unconverted CH₄ in the reducing gas. This carbon can be present in DRI as either cementite (Fe₃C) or free carbon (C_{free}); in conventional DRI, Fe₃C constitutes around 65–95% of the contained carbon and the amount of carbon ranges from 1.5% to 5.0% (by weight) [21,23,24]. The DRI carburization reactions can be summarized as [18,19,21,25]:



Note that: 1) reactions (5) and (6) are connected via the water-gas shift reaction; 2) reaction (5) is related to the well-known Boudouard reaction (2 CO → C + CO₂), which is catalyzed by metallic iron at temperatures above about 400 °C [24,26]. A high DRI carburization is advantageous in the EAF typically located downstream of the reduction shaft, helping to reduce any remaining FeO (FeO + C → Fe + CO) and decreasing the electricity demand of the melting process [23,26,27]. In addition, a high-carbon DRI is easier to handle and store due to its lower reactivity, particularly with air and H₂O, compared to low-carbon DRI.

An EAF is used to convert DRI, generally along with some amount of recycled steel scrap, to steel [18,28]. In the EAF, the DRI (or DRI-scrap mixture) is melted utilizing electricity that is fed via graphite (carbon) electrodes. This melting is an electricity-intensive process, despite the fact that a substantial share of the energy demand – typically around 35–60% – is provided by the oxidation of elements (foremost carbon) in the DRI or DRI-scrap mixture [23,29]. Part of this oxidation is

customarily achieved via oxygen injection into the EAF; natural gas or oil burners can also provide part of the energy demand [29,30]. Process CO₂ emissions from the EAF stem from oxidation of carbon in the DRI or scrap (or injected carbon fines), combustion of natural gas or oil, or consumption of the graphite electrodes [29]. During the melting process, impurities originating from the iron ore, most notably phosphorous and sulfur, are simultaneously removed through a slag. The formation of this slag is facilitated by the addition of lime to the EAF [31].

As mentioned, the reducing gas of DR processes is most often generated via the reforming of natural gas. The three main reforming processes applied in conventional DR processes are [19]:

1. External steam reforming: a conventional steam reformer is used to produce a H₂-CO mixture via a reaction between natural gas and a stoichiometric excess of H₂O over a catalyst; the HyL III process is an example of a DR process that utilizes this type of reforming [18,22,32,33].
2. External top gas reforming: the top gas, i.e., the gas that leaves the top of the reduction shaft, is recycled back to the reformer. In the reformer, part of the formed H₂O and CO₂ react with fed natural gas over a catalyst, producing H₂ and CO. This type of DR process, also known as the MIDREX process, is seen in Fig. 1 [20,34].
3. Internal reforming: natural gas is directly fed to the reduction shaft, in which the iron acts as a reforming catalyst [20,34,35]. A separate reformer is not necessary in this design. This type of process is seen in Fig. 2. The HyL/Energiron ZR process is an example of this type of scheme [30,33,35].

As can be seen in Figs. 1 and 2, the top gas is recycled back to the reformer or pre-heating section in both processes, with some of the top gas being combusted to provide heat. In the case of external top gas reforming, a large share of the top gas can be recycled as both H₂O and CO₂ is consumed in the reforming process, although a part of the top gas is combusted to provide heat. In contrast, it is necessary to selectively remove H₂O and CO₂ from the top gas in the internal reforming process to prevent their accumulation [28].

1.2. Hydrogen direct reduction

Unlike the conventional DR process described above, an H-DR

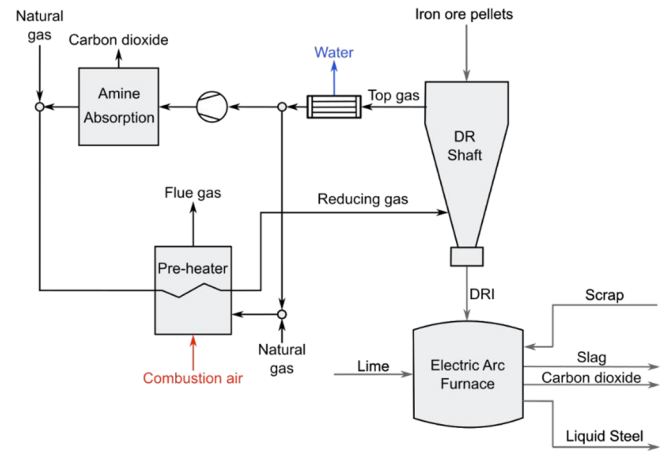


Fig. 2. Internal reforming direct reduction process [36].

process is based on a feed of pure H₂, typically suggested to be provided by the electrolysis of water, rather than natural gas [7,37,38]. This theoretically leads to a somewhat less complex process as there are no carbonaceous species present in the reduction shaft. Moreover, as no CO is consumed in reduction reactions and no fossil natural gas is combusted, process CO₂ emissions should be minimal [1]. Heating of the reducing gas should preferably not be achieved via combustion of H₂ due to the relatively low efficiency; electric heating is one suitable alternative [27,39,40]. A process scheme of a H-DR process featuring electric reducing gas pre-heating is seen in Fig. 3.

2. Suggested methanol-based direct reduction process

A CH₃OH-based H₂ storage system could be integrated into an H-DR process in several ways. Here we assess one possible CH₃OH-based DR process based on the incorporation of a high-temperature electrolyzer and a biomass oxy-fuel furnace, as seen in Fig. 4. In contrast to conventional DR processes based on a feed of fossil natural gas, this process is powered by electricity and biomass, which allows for fossil-free steelmaking. An advantage of the suggested DR process over the H-DR process seen in Fig. 3 is the possibility to produce carburized DRI.

The suggested process can be divided into steady-state and dynamic

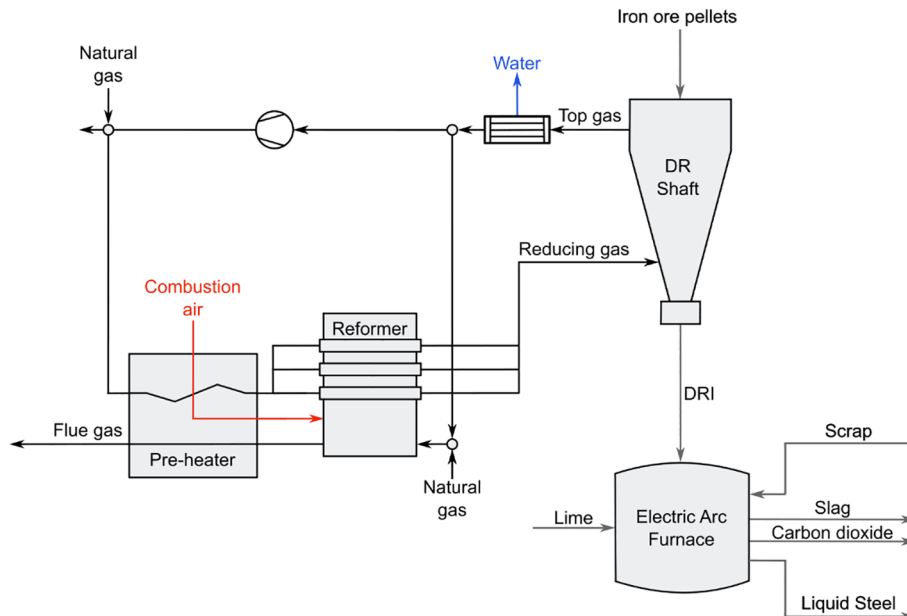


Fig. 1. External top gas reforming direct reduction process [20].

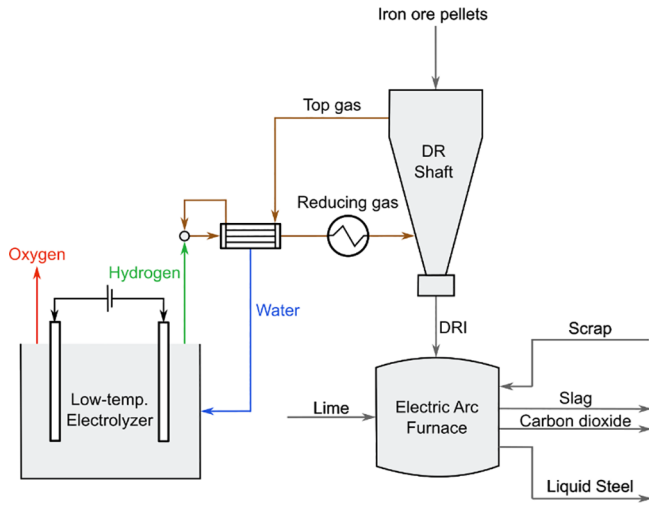


Fig. 3. Generic hydrogen direct reduction process.

parts. The dynamic part of the process is made up of the low-temperature electrolyzer, the CH_3OH production process, the CH_3OH storage, and the CH_3OH reformer with the associated gas separation step, here assumed to be pressure swing adsorption (PSA). The purpose of the dynamic part of the process is to deliver a constant stream of H_2 to the reduction shaft at as low cost as possible, where that cost is largely determined by the price of electricity used to operate the low-temperature electrolyzer. During times of relatively low electricity prices, the low-temperature electrolyzer is operated at or near its maximum load, delivering all H_2 to both the reduction shaft and the CH_3OH production process, which is also operated at its maximum load. Conversely, during times of relatively high electricity prices the low-temperature electrolyzer is operated at its minimum load, delivering only as much H_2 as is necessary to operate the CH_3OH production process at its minimum load. To compensate for the then lower H_2 production from the low-temperature electrolyzer, stored CH_3OH is

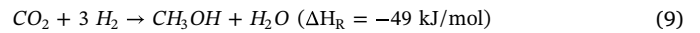
consumed to produce H_2 and CO_2 in the CH_3OH reformer. The CO_2 formed in the reforming process may be recycled back to the high-temperature electrolyzer or the CH_3OH production process. Note that the production of CH_3OH also depends on the degree of filling of the CH_3OH storage.

The steady-state part of the process consists of all remaining units, centered around the reduction shaft and the delivery of reducing gas. The reducing gas delivered to the reduction shaft is a mixture of three gas streams: 1) H_2 from the dynamic part of the process, i.e., the low-temperature electrolyzer or CH_3OH reformer; 2) recycled top gas that has had most H_2O and CO_2 removed via condensation and amine absorption, respectively; and 3) H_2 and CO from the high-temperature electrolyzer. The CO_2 captured from the top gas is recycled back to the rest of the process for conversion to CO or CH_3OH .

As the overall reduction-carburization process inside the reduction shaft is endothermic, it is necessary to pre-heat the entering reducing gas so that sufficient reaction rates are achieved. The incoming reducing gas is first pre-heated via heat exchange with the top gas. Thereafter, further heat is provided via the oxy-fuel combustion of biomass. The oxy-fuel combustion also provides carbon in the form of CO_2 to the process to produce CH_3OH or CO and make up for any carbon consumed by DRI carburization. It is assumed that it is not possible to reach a sufficiently high reducing gas temperature via heat exchange with the oxy-fuel flue gas due to material constraints [41]. Therefore, the final pre-heating of the reducing gas up to the reduction shaft temperature is achieved via electric heating.

2.1. Methanol production from carbon dioxide

Conventional CH_3OH production processes are based on a feed consisting of predominately H_2 and CO with small amounts of CO_2 [42]. However, it is also possible to produce CH_3OH via the direct reaction of CO_2 and H_2 according to the following reaction [43]:



As CO_2 must be separated out from the DR process top gas, as seen

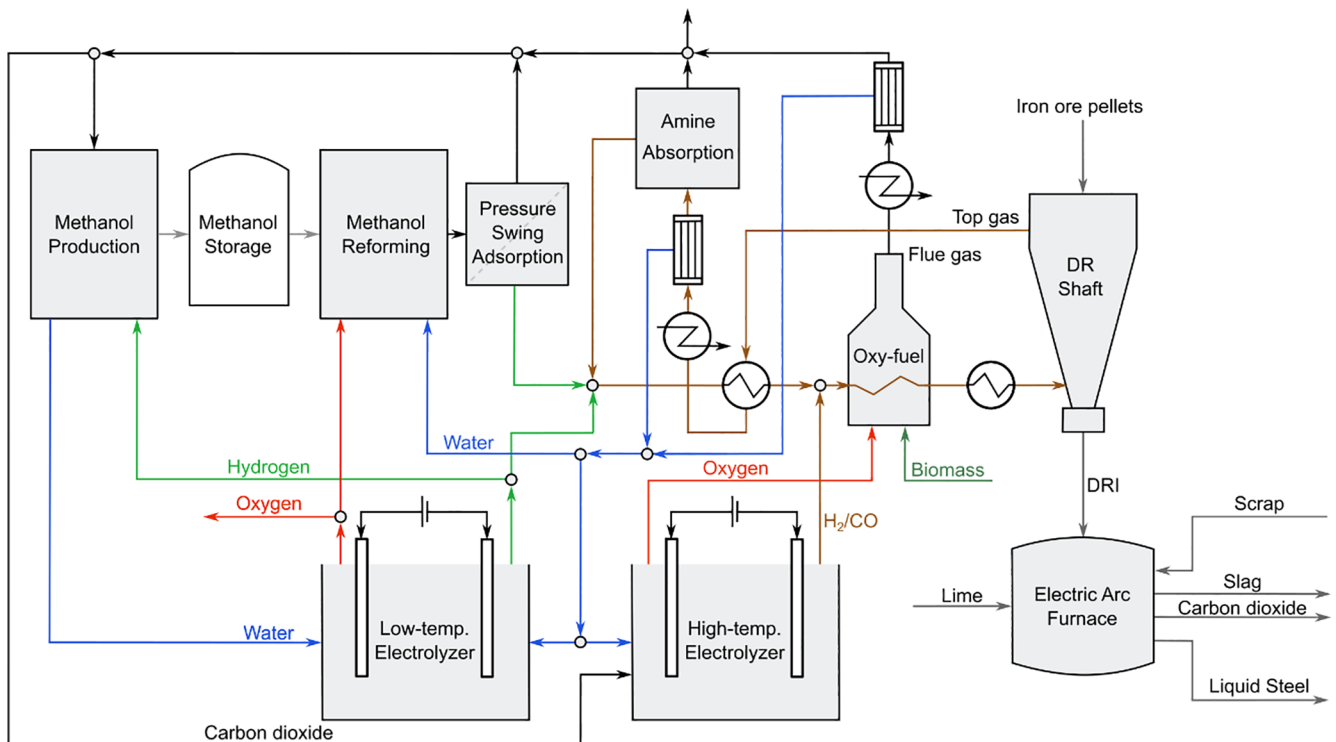


Fig. 4. Suggested methanol-based direct reduction process (DR: direct reduction).

in Fig. 4, the reaction above becomes a convenient way to store H_2 (and CO_2) in liquid form in the context of a DR process. The basic process of producing CH_3OH from CO_2 and H_2 , as seen in Fig. 5, consists of feed and recycle compressors, a (series of) reactor bed(s), and a distillation section, which may consist of one to four distillation columns depending on the target CH_3OH purity [44]. As the CH_3OH -forming reaction is exothermic, it is necessary to cool the reactor(s), either via a series of heat exchangers (as in Fig. 5) or via quench streams (multiple reactant inlets along the length of the reactor), to achieve sufficient conversion per reactor pass [45]. The same type of catalyst can be used in the CO_2 -based process as in the conventional CH_3OH production process and in CH_3OH reforming: $Cu/ZnO/Al_2O_3$ [46]. Typical reactor conditions are 210–280 °C at 40–80 bar. The presence of the recycle stream necessitates a purge stream to avoid the accumulation of inert gases in the system. The purge stream is small, about 1% (by mole) of the recycle stream is sufficient, and is combusted to provide additional heat [47–49]. The heat generated via the CH_3OH -forming reaction and the purge combustion is sufficient to cover the heat demand of the distillation process [47,50]. Therefore, no external heat input is necessary in this process.

The electricity demand of the CH_3OH production process is mainly for the powering of compressors. Estimates of the electricity demand of larger-scale CO_2 -based CH_3OH production processes in the literature are typically in the range of 1–2 kWh/kg of stored H_2 (based on the storage of three moles of H_2 per mole of CH_3OH) [51,52], e.g., Perez-Fortes et al. estimated an electricity demand of 0.169 MWh/t CH_3OH for a plant producing 1320 t CH_3OH from CO_2 and H_2 per day, equivalent to, considering the stoichiometry of reaction (9), 0.9 kWh/kg H_2 stored in CH_3OH [47].

Conventional CH_3OH plants typically operate at steady state. In the case of the DR process suggested here, a flexible CH_3OH production process is necessary since the main purpose of the H_2 storage is to compensate for variable electricity prices. Recent literature indicates that such dynamic operation of a CH_3OH production process may be achievable, with a minimum load of 20% of the maximum capacity [53–58], although certain CO_2 -based CH_3OH production process equipment suppliers have claimed that even lower minimum loads are attainable [59,60]. Nevertheless, no such dynamic CH_3OH production process has yet been realized on an industrial scale, presumably because conventional plants have been based on a steady feed of natural gas or coal [54].

2.2. Supply of carbon and heat to the process

When carbon-containing DRI is produced it is necessary to supply carbon to the DR process, and if the process should be fossil fuel-independent this carbon should originate from biomass. The minimum amount of carbon that must be supplied to a DR process can be estimated by considering the DRI production and its degree of carburization. At a production of 2 Mt DRI per year, approximately equal to the current steel slab production at the SSAB BF-BOF plant in Luleå [61], and a degree of carburization of 1% (by weight), the carbon consumption of the process is 20 000 t per year, equivalent to a minimum supply of around 73 000 t of CO_2 per year, considering stoichiometry. The amount of biogenic CO_2 available from higher-concentration sources in Sweden, such as biofuel production processes, is considerably less [62]. Accordingly, we consider it most likely that carbon must be supplied to the DR process via a direct influx of biomass to the site.

As large amounts of heat also must be provided to the DR process, we regard the oxy-fuel combustion of biomass the most suitable option for this supply of carbon. The principle of oxy-fuel combustion is simple: instead of combusting a fuel in air, O_2 is used as the oxidant. The avoidance of N_2 in the oxidant stream results in a flue gas consisting of mostly steam and CO_2 , from which the CO_2 can easily be separated via condensation of the steam [63]. In conventional oxy-fuel combustion processes, the generation of near-pure O_2 using an air

separation unit (ASU) is a significant thermodynamic and economic obstacle [64]. In the here suggested DR process there are already large amounts of O_2 available from the electrolyzers. This pure O_2 may thus be used directly in the oxy-fuel combustion process, as seen in Fig. 4, without additional costs.

2.3. Production of reducing gas in a methanol-based direct reduction process

2.3.1. Electrolysis

The production of H_2 from H_2O electrolysis provides a possible route to fossil-free H_2 . Table 1 gives a brief comparison of current commercial electrolyzer technologies. Alkaline electrolysis (AEL) is the most mature technology with operational lifetimes of 10 to 20 years. Proton exchange membrane electrolysis (PEMEL) has recently become a possibly viable alternative to AEL. PEMEL can operate at higher current densities than AEL, enabling a more compact design, and go up and down in load more rapidly, although both technologies can operate in wide load windows [65,66]. Both AEL and PEMEL are characterised as low-temperature electrolysis technologies as both operate below 100 °C, i.e., on liquid H_2O .

In contrast to AEL and PEMEL, solid oxide electrolysis (SOEL) is a high-temperature technology, i.e., it operates on steam and not on water (typically at 700–1 000 °C). SOEL is more efficient than low-temperature technologies, but is associated with higher investment costs. High-temperature electrolysis is particularly interesting when external heat, or steam, is available as this avoids the need for supply of the heat of evaporation of H_2O . A potentially attractive operating mode for SOEL is the production of a mixture of H_2 and CO (syngas) when steam and CO_2 are co-fed; this concept is referred to as co-electrolysis. The molar ratio of H_2 and CO can be tailored depending on the requirement of the product syngas. Such co-electrolysis of H_2O and CO_2 could provide a one-step fossil-free method for producing both H_2 and CO in a DR process.

As one mole of H_2 or CO can reduce the same amount of Fe_2O_3 (per reactions (1) and (2)), the electricity consumption per mole of CO and H_2 is of particular importance for a DR process. In addition to H_2 and CO , CH_4 is also formed as a side product when operating an SOEL in co-electrolysis mode [70]. However, current literature reveals that operating the SOEL at high temperatures and low pressures inhibits CH_4 production [71].

2.3.2. Methanol reforming

The release of H_2 from CH_3OH can be achieved via four reactions: 1) endothermic steam reforming (SR); 2) exothermic partial oxidation

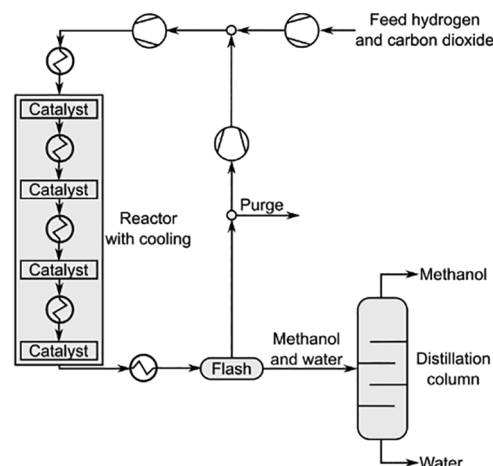


Fig. 5. The basic layout of a CO_2 -based CH_3OH production process [50].

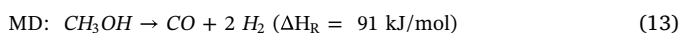
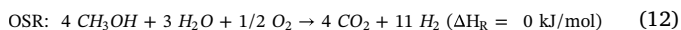
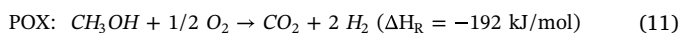
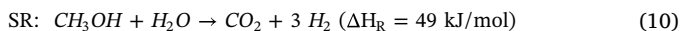
Table 1
Operational data for current commercial electrolyzer technologies [66–69].

	AEL	PEMEL	SOEL
Temperature (°C)	60–90	50–80	700–1 000
Pressure (bar)	10–30	20–50	1–15
Current density (A/cm ²)	0.25–0.45	1.0–2.0	0.3–1.0
System efficiency ^a (%)	51–60	46–60	76–81
Specific energy consumption ^b (kWh/Nm ³)	5.0–5.9	5.0–6.5	3.7–3.9
Lifetime (kh)	55–120	60–100	8–20
Capital expenditure (€/kW _{el})	1 000–1 200	1 860–2 320	> 2000

^a Electricity demand, including auxiliaries and heat supply, on a lower heating value basis starting from liquid water.

^b System level.

(POX); 3) oxidative steam reforming (OSR); and 4) endothermic CH₃OH decomposition (MD):



The OSR reaction is a combination of the SR and POX reactions. For certain ratios of fed O₂ and H₂O, the OSR reaction is heat-neutral, excluding pre-heating of the reactants up to the reactor temperature; this is referred to as autothermal reforming. The methanol reforming reactions are typically performed over a Cu/ZnO/Al₂O₃ catalyst [72–74]. It should be noted that the evaporation of CH₃OH and H₂O constitutes most of the heat demand of the SR and OSR processes. Therefore, it is highly advantageous if steam and gaseous CH₃OH can be delivered to the reforming process. For instance, if liquid H₂O and CH₃OH is delivered to an OSR operating at autothermal conditions, the minimum amount of H₂ that must be combusted to provide heat for the process increases from 7 to 15% of the released H₂.

The MD reaction is noteworthy in the present context as it directly produces a mixture of H₂ and CO, similar to the reducing gas of conventional DR processes. Furthermore, although the yield of H₂ is lower in MD than in OSR or SR, MD produces one equivalent of CO, which has the same theoretical reduction capacity as H₂ and may also be used for carburization. Notable disadvantages of the MD reaction are the high endothermicity and the likely increased formation of byproducts such as methyl formate, CH₄, and dimethyl ether [75]. MD suffers from several uncertainties at the present conceptual stage and is therefore not considered further.

Another reforming option of interest is to directly utilize the top gas, specifically its H₂O and CO₂ content, in the reformer. However, it is presently unclear whether the reforming of CH₃OH with CO₂, i.e., dry reforming of CH₃OH, is viable. Therefore, like with the internal reforming approach, we do not pursue the dry reforming of CH₃OH further here. POX is not pursued further either due to the low H₂ yield and

the intermittent generation of large amounts of heat. However, the continuous POX of small amounts of CH₃OH may be an attractive option to increase the reducing gas temperature before the reduction shaft, analogous to the common practice of POX of CH₄ in conventional DR processes [19].

The remaining CH₃OH reforming options, i.e., SR and OSR, do each have specific advantages when integrated into a CH₃OH-based DR process. One critical factor is the heat demand of the processes: starting from liquid H₂O and CH₃OH at room temperature, SR demands approximately twice the heat of OSR when operated in autothermal mode. The price of the reduced heat demand of OSR is met by the loss of H₂ in the process, approximately 8% compared to SR per the stoichiometry of reaction (12). As this lost H₂ would originally be produced from electricity, the choice between OSR and SR is ultimately decided by the relative costs of electricity and heat. An advantage of the OSR route is that the addition of O₂ inside of the reactor allows for very efficient heat transfer, allowing fast start-up times and rapid response to changes in reformer load [73,76]. However, at present time it is difficult to evaluate the value of a more dynamic operation of the reforming process.

2.4. Capture of carbon dioxide from top gas

As produced CO₂ is not consumed, it is necessary to selectively remove CO₂ from the top gas to prevent its accumulation in the reduction shaft recycle loop (as seen in Fig. 4). While many CO₂ removal technologies are possible, e.g., adsorption, membranes, molecular sieves, and cryogenic separation, the only technology that has been successfully applied in conventional DR processes is amine absorption [28,77,78]. Absorption-based CO₂ separation processes are suitable for the removal of CO₂ from DR process top gas since: 1) the partial pressure of CO₂ in the top gas is typically low (below 20% (by mole)), a detriment to CO₂ separation methods based on compression; and 2) any suitable surplus heat from the DR process may be used to regenerate the amine solution [79,80].

The most common solvents for absorbing CO₂ are aqueous monoethanolamine (MEA) solutions (20–30% MEA (by weight)) [77,81]. The generation of low-pressure steam for the regeneration of the amine solution at 100–120 °C constitutes the major part of the energy demand of MEA CO₂ absorption processes with steam demands typically in the range of 3–4 MJ/kg CO₂ [81].

3. Method and assumptions

The basic mass and energy balances of the suggested CH₃OH-based DR process were calculated to evaluate its feasibility and performance, e.g., its heat and electricity use, and how much H₂ that can be stored in the form of CH₃OH per day. It was found necessary to adopt several assumptions and simplifications to perform these calculations. A major reason for this need for simplification is the currently large number of uncertainties regarding the process components and their interconnections. Therefore, the results of these calculations should be

Table 2
Shomate equation parameters for relevant gases [82].

Compound	H ₂		CO	H ₂ O(g)	CO ₂	O ₂	
Temperature (K)	298–1 000	1 000–2 500	298–1 300	500–1 700	298–1 200	100–700	700–2 000
A	33.066178	18.563083	25.56759	30.092	24.99735	31.32234	30.03235
B	−11.363417	12.257357	6.09613	6.832514	55.18696	−20.2353	8.772972
C	11.432816	−2.859786	4.054656	6.793435	−33.69137	57.86644	−3.988133
D	−2.772874	0.268238	−2.671301	−2.53448	7.948387	−36.5062	0.788313
E	−0.158558	1.97799	0.131021	0.082139	−0.136638	−0.00737	−0.741599
F	−9.980797	−1.147438	−18.0089	−250.881	−403.6075	−8.90347	−11.32468
G	172.70797	156.288133	227.3665	223.3967	228.2431	246.7945	236.1663
H	0	0	−110.5271	−241.8264	−393.5224	0	0

considered as basic estimates based on a conceptual process design. Calculations were performed in MS Excel using the built-in solver tool. Specific heat capacities and enthalpies of gases were calculated using the Shomate equation (Eqs. (14) and (15)) using parameters from the National Institute of Standards and Technology (NIST) Webbook per Table 2 [82]:

$$c_p^\circ = A + B \cdot t + C \cdot t^2 + D \cdot t^3 + \frac{E}{t^2} \quad (14)$$

$$H^\circ - H^\circ_{298.15} = A \cdot t + B \cdot t^2/2 + C \cdot t^3/3 + D \cdot t^4/4 - E/t + F - H \quad (15)$$

where c_p° is the specific heat capacity (in J/(mol, K)), t the temperature ($t = T/1000$, where T is the temperature in Kelvin), and H° the specific standard enthalpy (in kJ/mol). The reference state for enthalpy calculations is 25 °C, 1 bar, and $H_2O(g)$.

The iron ore pellets that are fed to the reduction shaft are anticipated to consist of Fe_2O_3 and 5% (by weight) of inert material [7]. This inert material remains as part of the produced DRI and is later separated out in the EAF as slag. A DRI metallisation of 94% is assumed in all cases; all remaining iron oxide is in the form of FeO , as is typical in conventional DRI production [17,23]. Consequently 25.4 kmol of reductant, i.e., H_2 or CO , is consumed per t DRI per equation (16), considering the stoichiometry of reactions (1), (2), (3), and (4):

$$\dot{n}_{red} = \left(X_{Fe} \cdot \frac{3}{2 \cdot M_w(Fe)} + (1 - X_{Fe}) \cdot \frac{1}{2 \cdot M_w(FeO)} \right) \cdot 10^3 \quad (16)$$

where X_{Fe} is the weight fraction of Fe in the DRI (excluding inert material), $M_w(Fe)$ the molar weight of Fe, and $M_w(FeO)$ the molar weight of FeO . The weight fraction of Fe in the DRI can be calculated using the DRI metallisation (M) per equation (17). A DRI metallisation of 94% yields $X_{Fe} = 0.92$.

$$X_{Fe} = \frac{M_w(Fe)}{M_w(Fe) + M_w(FeO) \cdot \left(\frac{1}{M} - 1 \right)} \quad (17)$$

The radiation and convection losses from the reduction shaft is assumed to be 15% of the thermal energy of the entering reducing gas (calculated per Eq. (15) for the various components) [83]. All solids passing through the reduction shaft are assumed to have a heat capacity of 0.56 kJ/(kg, K) and to enter and exit the reduction shaft at temperatures of 25 °C and 850 °C, respectively [83]. As the mass of carbon in the produced DRI is relatively small in all cases, the difference in DRI mass caused by carburization is ignored in the energy balance over the reduction shaft. The production of DRI (excluding inert material and carbon, i.e., only Fe and FeO) is assumed to be 2 Mt per year with the plant is in operation for 360 days per year, which is taken as the standard plant utilization. This yields the solid-phase reduction shaft mass balance in Table 3:

Assuming that all Fe in the produced DRI ends up in the final steel product and that all inert material is separated out as slag in the EAF, this yields 1.97 Mt liquid steel (Fe) per year. The plant, excluding the CH_3OH production process and the steam fed to the high-temperature electrolyzer and the amine-based CO_2 absorption process, is assumed to operate at atmospheric pressure [7].

Due to equilibrium reasons, only part of the H_2 and CO in the reducing gas entering the reduction shaft is consumed per pass. A per-pass conversion of 30% of entering H_2 and CO is assumed for the reduction reactions, based on the modelling work of Yi et al. [84]. However, it is assumed that all H_2 and CO sent to the reduction shaft is eventually utilized upon sufficient recycling, i.e., there are no losses of H_2 or CO .

The effect of varying the H_2/CO ratio on the energy and mass balances of the process was investigated in the range of CO reducing gas concentrations of 5–30% (by mole) in increments of 5%. As the degree of carburization that is achieved under different process conditions is uncertain, this is considered a variable in the calculations with four cases (carbon by weight in DRI): 0.0%, 0.5%, 1.0%, and 1.5%. In

practice, a higher reducing gas CO concentration should enable a higher degree of carburization and vice versa [85]. Nevertheless, cases of high reducing gas CO content and low carburization or low CO content and high carburization are included to show all theoretical possibilities. In total, this yields 25 cases, per Table 4. Note that the case of 0.0% carburization and 0% CO in the reducing gas includes no high-temperature electrolysis or amine scrubber as no CO is supplied to the reduction shaft. Therefore, this is referred to as the H-DR case. The difference between this H-DR case and the process shown in Fig. 3 is the oxy-fuel pre-heating step and the CH_3OH -based H_2 storage.

For simplicity, it is assumed that all carbon in the DRI is in the form of Fe_3C , as most carbon is in conventional DR processes (especially for lower degrees of carburization [25]) and to be formed via reaction (5) [23]. Reaction (5) was chosen as this results in the largest CO_2 production per degree of carburization and, thus, represents a worst-case scenario as all produced CO_2 must be separated out to prevent its accumulation in the reactor loop. The CO consumed via carburization is assumed to be in addition to that consumed via reduction, i.e., the top gas flow is somewhat smaller for cases of higher carburization, even if the flow of reducing gas to the reduction shaft is identical in all cases.

It is assumed that a minimum temperature difference of 50 °C is achieved in the heat exchange between the top gas and the reducing gas. The reducing gas, excluding additions of H_2 and CO from the high-temperature electrolyzer, is assumed to enter this heat exchanger at 70 °C. The remaining heat in the top gas after this heat exchanger down to 140 °C is used to generate part of the 3 bar steam (saturation temperature 133.5 °C; only heat of vaporization (2163.5 kJ/kg H_2O) is considered [86]) needed for the regeneration of the amine solution. Thereafter the top gas is cooled down further (to around 50 °C) to condense steam and to facilitate the subsequent CO_2 absorption process [77,87,88]. The low-temperature heat generated by this cooling and condensation is not utilized in the current system. However, it is possible that it could be used to provide e.g., district heating. The CO_2 absorption process is modelled as a black box process and is taken to require an input of 3.5 MJ/kg CO_2 of 3 bar steam for regeneration of the amine solution [81]. The reducing gas is assumed to always contain 5% CO_2 and 5% of H_2O (by mole) due to their incomplete separation from the top gas. However, to maintain the same reducing gas flow in the pure H-DR case (with no CO) as in all other cases, it is assumed that the reducing gas then contains 90% H_2 and 10% H_2O (by mole).

The low-temperature electrolyzer is assumed to be of the AEL kind and to require 50.0 kWh of electricity per kg of H_2 (100.8 kWh/kmol H_2) independently of its load; this efficiency is based on projected values for 2030 [67,89]. The high-temperature electrolyzer is of the SOEL kind and operates in H_2O - CO_2 co-electrolysis mode. The SOEL operates at 700 °C, producing a 1:1 M ratio of H_2 and CO at an electricity demand of 70 kWh/kmol of reductant when receiving saturated steam at 3 bar (starting from $H_2O(l)$ at 25 °C and 1 bar, this is equivalent to a heat demand of 13.1 kWh/kmol, yielding a total energy demand of SOEL of 83.1 kWh/kmol). The electricity consumption of the SOEL is estimated via simulations; further details can be found in literature [71,90–93]. The high-temperature electrolyzer is assumed to operate at atmospheric pressure; consequently CH_4 formation is most likely negligible and thus neglected [71,94].

The biomass combusted in the oxy-fuel furnace is taken to have an elementary dry composition of 51% carbon, 6% hydrogen, and 43%

Table 3
Mass balance for solids in the reduction shaft.

Component	In (t/h)	Change (t/h)	Out (t/h)
Fe_2O_3	325.4	−325.4	0
Inert solids	17.1	0	17.1
FeO	0	+17.6	17.6
Fe	0	+213.9	213.9
Sum	342.5	−93.9	248.6

Table 4
Studied cases of reducing gas CO concentration and DRI carburization.

Reducing gas CO concentration (% by mole)	0.0% carburization (by weight)	0.5% carburization (by weight)	1.0% carburization (by weight)	1.5% carburization (by weight)
0	Yes (H-DR case)	No	No	No
5, 10, 15, 20, 25, 30	Yes	Yes	Yes	Yes

oxygen (by weight) and to carry with it 50% (by weight) liquid H₂O [95]. The higher heating value (HHV) of the dry biomass is 19.4 MJ/kg of moisture- and ash-free substance (MAF), yielding a lower heating value (LHV) of 17.0 MJ/kg MAF [95]. The biomass is assumed to be completely combusted (i.e., all hydrogen in the fuel is converted to H₂O and all carbon in the fuel is converted to CO₂) in the oxy-fuel furnace at a stoichiometric excess of O₂ of 10% (by mole). The O₂ necessary for the combustion is delivered from the process electrolyzers and is assumed to enter at a temperature of 25 °C. A cold-side temperature of 700 °C is achieved in the oxy-fuel reducing gas pre-heating step. Any remaining heat in the oxy-fuel flue gas after this heat exchange with the reducing gas down to 140 °C is used to generate 3 bar steam. An exception is the H-DR case, where there is no demand for 3 bar steam. Here a minimum temperature difference of 50 °C is achieved already during heat exchange with the reducing gas. The efficiency of heat transfer from the oxy-fuel combustion is assumed to be 90%.

After heat exchanging, the H₂O in the oxy-fuel flue gas is condensed and separated out, leaving a stream of essentially pure CO₂. It is assumed that this CO₂ is sufficiently pure to be sent directly to the CH₃OH production process, i.e., the energy demand of any additional gas cleaning steps is assumed to be negligible. As with the top gas condenser, the condensation heat could be (but is in the current system not) used for district heating. The final pre-heating of the reducing gas from 700 °C up to the reduction shaft temperature of 900 °C is achieved by electrical heating with an efficiency of 100%. As no carbon is consumed in the H-DR case, it is then principally possible to operate the process on electric pre-heating alone if desired, as seen in Fig. 3.

The CH₃OH production process is assumed to require an input of 1 kWh/kg of H₂ stored in CH₃OH for compression purposes [47]. The internal heat demand of this process, including distillation, is assumed to be entirely covered by the reaction heat, i.e., there is no need to supply external heat. Only the stoichiometry of reaction (9) is considered; formation of side products is assumed to be unimportant for the overall mass and energy balances [49]. The identification of the maximum allowable CH₃OH production capacity is a goal of the presented energy and mass balances.

The heat demand of the CH₃OH reformer, also modelled as a black box process, is estimated based on the use of either SR (reaction (10)) or OSR (reaction (12)) using the enthalpies of vaporization of H₂O (40.66 kJ/mol) and CH₃OH (35.20 kJ/mol) at their respective standard boiling points. Assuming a stoichiometric excess of H₂O of 50% is utilized in SR yields [96]:

$$\text{Heat demand}_{\text{SR}} = \frac{\Delta H_{\text{R,SR}} + 1.5 \cdot \Delta H_{\text{vap,H}_2\text{O}} + \Delta H_{\text{vap,CH}_3\text{OH}}}{(\text{mol H}_2 / \text{mol CH}_3\text{OH})_{\text{SR}}} = 48.4 \text{ kJ/mol H}_2 \quad (18)$$

$$\text{Heat demand}_{\text{OSR}} = \frac{\Delta H_{\text{R,OSR}} + (3/4) \cdot \Delta H_{\text{vap,H}_2\text{O}} + \Delta H_{\text{vap,CH}_3\text{OH}}}{(\text{mol H}_2 / \text{mol CH}_3\text{OH})_{\text{OSR}}} = 23.9 \text{ kJ/mol H}_2 \quad (19)$$

Note that approximately 8% of H₂ in CH₃OH is lost as heat in the OSR case, per stoichiometry. The EAF is assumed to be fed by only hot DRI, resulting in an electricity demand that varies linearly with the DRI carburization between 760 kWh/t steel for carbon-free DRI and 520 kWh/t steel for DRI with a carburization of 2% (by weight) (1.5% is the highest DRI carburization considered here) [8]. No addition of steel scrap to the EAF is considered.

The basic calculations performed in this article considers only the

basic chemical and physical processes occurring in the different parts of the process using e.g. stoichiometry, heat capacities, and reaction enthalpies. More complex aspects, such as the kinetic effects in the reduction shaft and changes in the energy demand of various sub processes due to variations in load, have been left out. Furthermore, the energy demand of certain minor parts of the process, such as CO₂ purification as part of the oxy-fuel process, H₂O purification processes, and pumping of liquids have been neglected in the calculations.

4. Results and discussion

4.1. Mass balances

The currently available data on the mass balance of a conventional DR shaft for varying reducing gas compositions is limited [14,34,97,98]. This lack of available data means that it is not possible to validate the simple reduction shaft model applied here for all considered conditions. Nevertheless, the developed simplified reduction shaft model does correspond well with actual MIDREX plant data for similar reducing gas conditions, as seen in Table 5.

An important aspect of the suggested CH₃OH-based DR process is the carbon mass balance: the amount of CO₂ delivered by the oxy-fuel combustion process and separated out from the top gas must be sufficient for the operation of the high-temperature electrolyzer. As seen in Fig. 6 for degrees of carburization of 0.0% (left) and 1.5% (right), this condition is fulfilled for all considered conditions (this also applies for intermediate degrees of carburization), i.e., there is always an excess of CO₂: the combined flow of CO₂ from the oxy-fuel furnace and the amine absorption unit (blue line) is larger than the consumption of CO₂ due to CO production for reduction and carburization via high-temperature electrolysis (green line) (note that the lines indicating total CO consumption (green line) and CO₂ separated from the top gas (yellow line) overlap in the 0.0% carburization case). This excess CO₂ can be used to store H₂ in CH₃OH. A consequence of this excess of CO₂ in the process is that it is not necessary to capture CO₂ from the downstream EAF, simplifying the overall process. When the CH₃OH reformer is operated there will always be a large excess of CO₂ as it is co-produced with H₂.

The relative excess of CO₂ is larger at lower CO concentrations in the reducing gas: in the case of 1.5% (by weight) DRI carburization presented in Fig. 6, the excess of CO₂ is (by mole) between 75% and 48% for CO concentrations of 5% and 30% in the reducing gas, respectively. Although the inflow of CO₂ from oxy-fuel combustion is higher at higher reducing gas CO content, this is outweighed by the

Table 5

Comparison of reduction shaft mass balance between the developed simplified model and data from Gilmore Steel Corporation MIDREX plant in Portland, Oregon, USA (production capacity: 26.4 t Fe/h) [14,98]. Gilmore plant DRI carburization: 2.0% (by weight), model carburization: 2.0% (by weight).

	Reducing gas (mol%)		Top gas (mol%)	
	Gilmore plant data	Model	Gilmore plant data	Model
H ₂	52	60	37	43
CO	30	30	19	18
CO ₂	5	5	14	16
H ₂ O	5	5	21	23
N ₂ + CH ₄	8	–	9	–

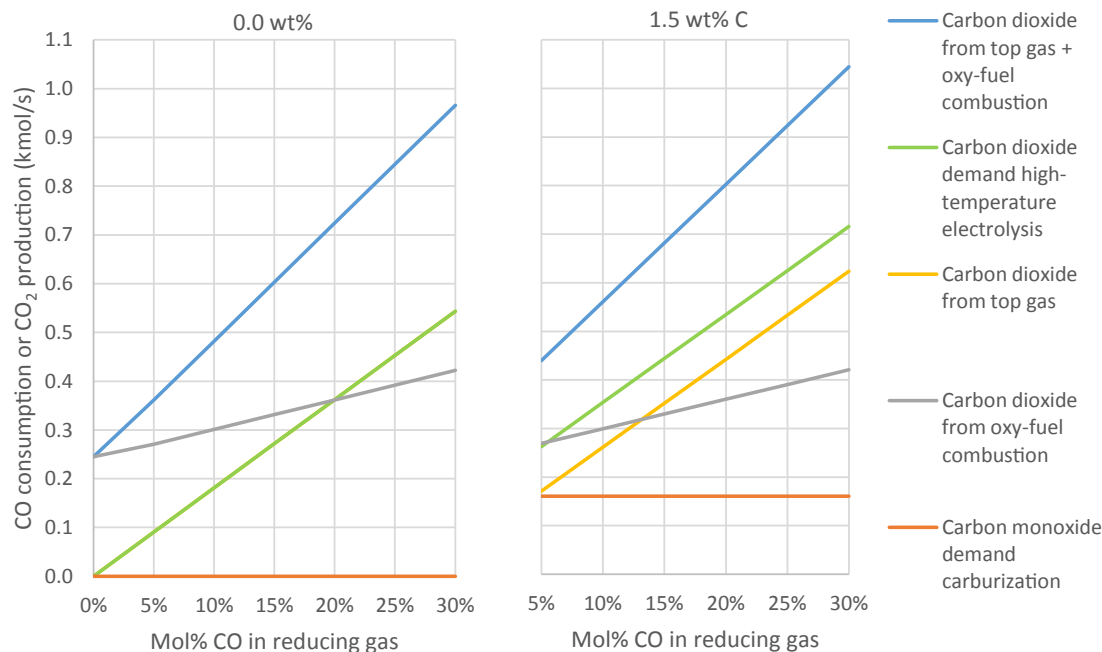


Fig. 6. Carbon mass balance for methanol-based direct reduction process; left: DRI carburization 0.0% (by weight), right: DRI carburization 1.5% (HT-el: high-temperature electrolysis).

increased CO₂ demand of the high-temperature electrolyzer. Note that although there is enough CO₂ supplied from only the oxy-fuel furnace to fully supply the process at low reducing gas CO concentrations, CO₂ must still be separated out from the top gas to prevent its accumulation. Therefore, it is not viable to separate out less CO₂ from the top gas when the excess of carbon in the system is high to decrease the heat demand.

As mentioned, the excess of CO₂ produced by oxy-fuel combustion and separated out from the top gas can be used to produce CH₃OH and store H₂. Accordingly, the data in Fig. 6 can be used to assess the allowed sizes of the CH₃OH production process and, thus, the low-temperature electrolyzer overcapacity, as this unit must supply sufficient H₂ for the CH₃OH production process. Assuming that each mole of excess CO₂ can be used to store three moles of H₂ (per reaction (9)), the maximum allowable overcapacity of the low-temperature electrolyzer

increases with increasing CO concentration in the reducing gas per Fig. 7. For pure H-DR (0% CO in reducing gas, 0% carburization, and with all CO₂ from the oxy-fuel combustion), the maximum overcapacity of low-temperature electrolyzers is approximately 267 MW, increasing to 471 MW for 30% (by mole) CO in the reducing gas (no carburization). These low-temperature electrolyzer overcapacities would allow for maximum CH₃OH production rates of between 244 and 431 kt/y. Increasing DRI carburization leads to lower allowable electrolyzer overcapacities as a higher share of CO₂ from oxy-fuel combustion must then be sent to the high-temperature electrolyzer for CO production. Accordingly, the case of 5% (by mole) reducing gas CO concentration and 1.5% (by weight) carburization achieves the lowest allowable overcapacity at 198 MW (equivalent to a maximum CH₃OH production rate of 181 kt/y).

Utilizing all of the available overcapacity for CH₃OH production is

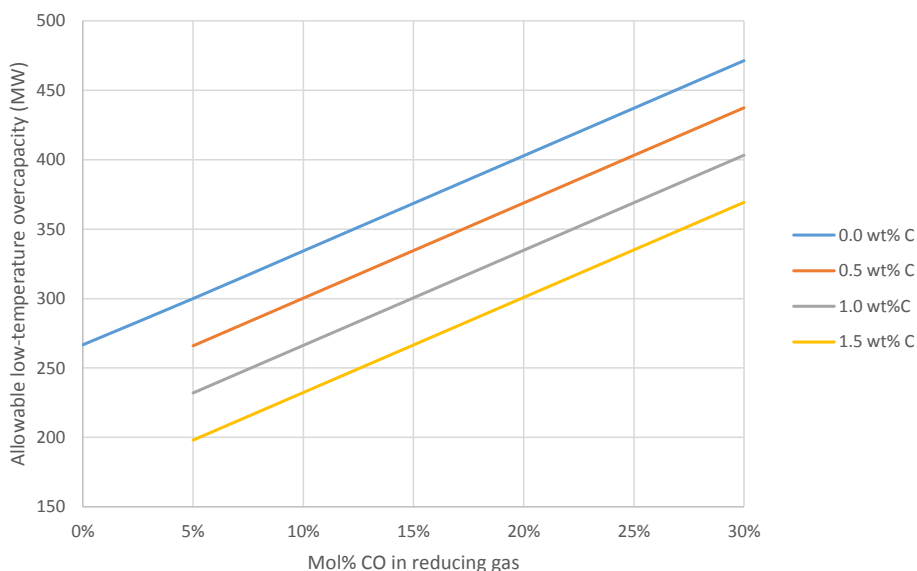


Fig. 7. Maximum allowable low-temperature electrolyzer overcapacity as a function of the concentration of CO in reducing gas for varying degrees of carburization.

likely not reasonable at higher reducing gas CO concentrations. In such a case, the minimum electricity demand of supplying the CH₃OH production process (at 20% load) with H₂ would nearly completely eliminate the possibility of dynamic operation of the process, i.e., reducing the electricity use during times of high electricity prices. This indicates that more venting of excess CO₂ may be necessary for higher reducing gas CO concentrations.

As the high-temperature electrolyzer is delivering a mixture of CO and H₂, a smaller share of the total H₂ will be delivered from the dynamic section of the process, i.e., the low-temperature electrolyzer or CH₃OH reformer, the higher the amount of CO in the reducing gas. This effect is seen in Fig. 8.

As can be seen, the share of the total H₂ that is delivered from the high-temperature electrolyzer increases rather rapidly with increasing reducing gas CO concentration. The effect of DRI carburization is also significant with higher shares of high-temperature electrolysis for higher degrees of carburization. As it is assumed that the flow of reducing gas is constant in all cases, more CO is consumed per pass for the cases of higher degrees of carburization and, thus, more H₂ is co-produced with this CO in the high-temperature electrolyzer. The share of H₂ being delivered from the high-temperature electrolyzer determines the maximum size of the CH₃OH reformer: the larger the share of H₂ that is delivered from the high-temperature electrolyzer is, the smaller the CH₃OH reformer has to be to cover the dynamic supply of H₂ to the reduction shaft.

It should be noted that there are sufficient amounts of O₂ delivered from the high-temperature electrolyzer to supply the oxy-fuel furnace for cases with high reducing gas CO concentrations and DRI carburization. For a DRI carburization of 1.5% (by weight), there is enough hot O₂ for the oxy-fuel furnace when the reducing gas CO concentration is higher than 8% (by mole). However, if the O₂ delivered from the high-temperature electrolyzer is not sufficient, O₂ from the low-temperature electrolyzer can be used as a supplement. The delivery of hot O₂ from the high-temperature electrolyzer would be advantageous for the oxy-fuel combustion energy balance, increasing the heat input per kg of MAF biomass by around 6% compared to when O₂ is delivered at 25 °C (as assumed in calculations).

4.2. Thermal energy balances

The presence of CO in the reducing gas decreases the heat demand of the reduction shaft due to the exothermic reduction (reaction (2)) and carburization (reaction (5)) reactions. This effect is seen in Fig. 9.

Clearly, the presence of CO in the reducing gas and carbon in the DRI has a substantial effect on the heat demand of the reduction shaft. A concentration of 30% (by mole) of CO in the reducing gas reduces the

heat demand of the shaft by 19% compared to the pure H-DR case, not considering carburization. The heat balance of the reduction shaft under different conditions is presented in Table 6.

The reduced heat demand of the reduction shaft at higher concentrations of CO in the reducing gas results in higher top gas heat temperatures. In the case of pure H-DR, our model results in a top gas temperature of 303 °C. For 30% (by mole) of CO in the reducing gas and a degree of carburization of 1.5% (by weight), the top gas temperature is 481 °C.

For the case of pure H-DR, the theoretical amount of pre-heating is 120 MW. In the case of a carburization of 1.5% (by weight) and a reducing gas CO concentration of 30% (by mole), the amount of reducing gas pre-heating is reduced to 80 MW due to the less exothermic operation of the shaft, out of which 40 MW is provided by oxy-fuel combustion. The amount of electrical heating necessary to provide the final pre-heating of the reducing gas from 700 °C to 900 °C is approximately 38 to 40 MW in all cases (small differences are due to variations in the reducing gas heat capacity), which corresponds to between 32% and 50% of the total amount of pre-heating. There are two additional major heat demanding sections of the process beyond the pre-heating of the reducing gas: the regeneration of the amine solution used for CO₂ capture and the generation of steam for the high-temperature electrolyzer. As the CO content in the shaft and DRI carburization increases, the heat demands of both of these processes increase, as seen in Fig. 10. However, part of this increase is compensated by the increase in excess heat in the top gas after heat exchange with the reducing gas that can be used to generate 3 bar steam.

The increased heat demand for CO₂ separation and steam generation outweighs the decrease in heat demand for pre-heating of the reducing gas. However, it should be noted that the heat necessary for the CO₂ separation process and the generation of steam for the high-temperature electrolyzer is of much lower temperature than that which is needed for the pre-heating of the reducing gas (mostly around 140 °C vs. from 300 to 400 °C up to 900 °C). Therefore, it is expected that oxy-fuel combustion can supply all of the necessary heat for these processes and, consequently, that no major additional amount of electrical heating is necessary. The utilization of waste heat from low-temperature electrolyzers via heat pumping may also be a viable option to provide this heat [99].

The maximum full load heat demand of the CH₃OH reformer (that is to be supplied intermittently) can be estimated by considering the enthalpies of the reforming reactions and the heats of evaporation of H₂O and CH₃OH per Eqs. (18) and (19). For SR, the maximum heat demand of the reformer is 79 MW, which is found in the H-DR case. If OSR is instead used, the maximum heat demand decreases to 39 MW. As the dynamic supply of H₂ decreases with increasing reducing gas CO

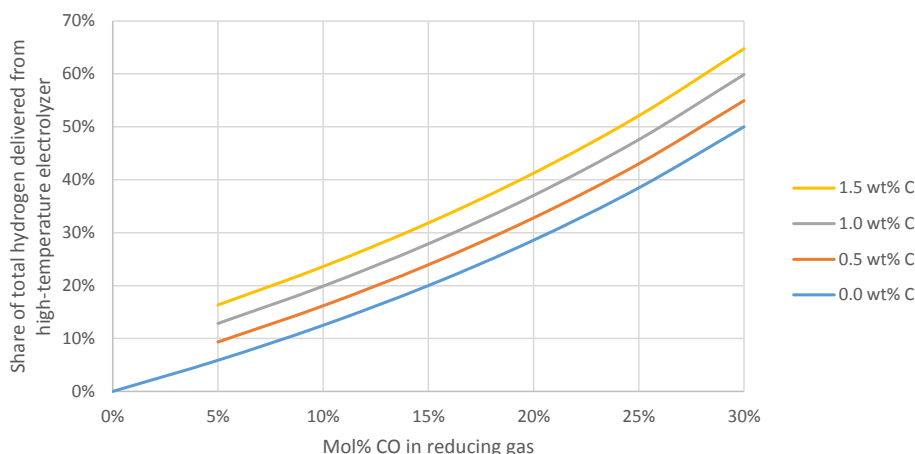


Fig. 8. Minimum share of total hydrogen delivered from high-temperature electrolyzer as a function of the concentration of CO in the reducing gas for varying degrees of carburization.

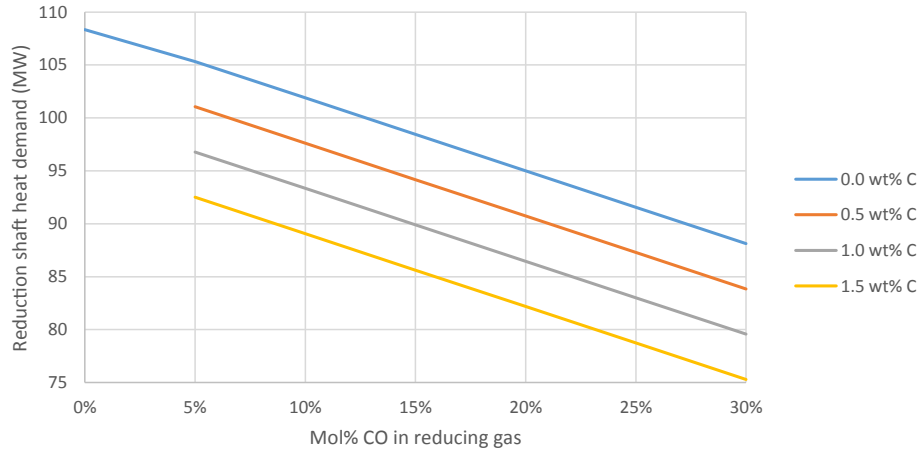


Fig. 9. Heat demand of reduction shaft as a function of the concentration of carbon monoxide in the reducing gas for varying degrees of carburization.

Table 6

Energy balance for reduction shaft in case of pure H-DR versus when CO is introduced. The reducing gas CO concentration has been chosen as to represent typical direct reduction processes for the case with carburization.

H-DR	Input	Heat (MJ/t DRI)	Share	Output	Heat (MJ/t DRI)	Share
	Reducing gas	2 334	100%	Heat of reactions	757	32%
				Sensible heat of DRI	462	20%
				Heat loss	350	15%
				Top gas	766	33%
	Total	2 334		Total	2 334	
30% CO in reducing gas, 1.5 wt% C in DRI.	Input	Heat (MJ/t DRI)	Share	Output	Heat (MJ/t DRI)	Share
	Reducing gas	2 417	100%	Heat of reactions	266	11%
				Sensible heat of DRI	462	19%
				Heat loss	363	15%
				Top gas	1 327	55%
	Total	2 417		Total	2 417	

concentration and DRI carburization, so does the reformer capacity and heat demand. For a reducing gas CO concentration of 30% (by mole) and a carburization of 1.5% (by weight), the maximum heat demand of the reformer is 18 MW for SR or 9 MW for OSR. It can be concluded that the share of the total heat demand of the DR process that must be intermittently supplied to the CH_3OH reformer is relatively small compared to the total heat demand of the process, especially for OSR and higher reducing gas CO concentration and DRI carburization.

4.3. Electricity demand

There are four major electricity demanding subprocesses in the investigated DR process: the low-temperature electrolyzer, the high-temperature electrolyzer, the EAF, and the final pre-heating of the reducing gas. The electricity demand of these processes is affected by changes in the reducing gas CO concentration and the DRI carburization.

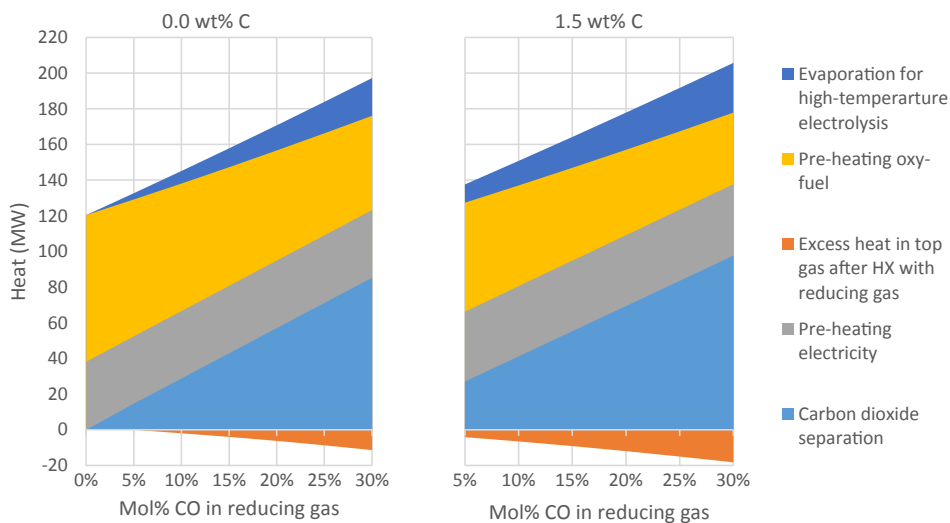


Fig. 10. Heat demand of direct reduction process based on reducing gas CO content (0.0% carbon (by weight) in DRI to the left and 1.5% carbon (by weight) to the right). Excess heat in top gas is used to generate 3 bar steam for regeneration of amine absorption solution and the high-temperature electrolyzer.

As seen in previous sections, the concentration of CO in the reducing gas affects the relative capacity of the low and high-temperature electrolyzers. The degree of carburization mainly affects the electricity demand of the EAF downstream the reduction shaft. The electricity demand of the reducing gas pre-heating process does not change significantly when varying the reducing gas CO content, as the temperature of the reducing gas after heat exchange with the oxy-fuel flue gas is assumed to be the same in all cases. The effect of changing the reducing gas CO content and the degree of carburization on the electricity demand of the DR process is shown in Fig. 11. Note that any low-temperature electrolyzer overcapacity is excluded, i.e., the shown electricity demand is for the case that electrolyzers provide all of the reducing gas. Likewise, the electricity demand of the CH₃OH production process is not included as its optimal capacity is unknown. However, even for the maximum allowable CH₃OH production capacities, its contribution is relatively small (under 10 MW at maximum load in all cases).

In Fig. 11, it is seen that the overall electricity demand decreases with increasing reducing gas CO concentration and DRI carburization. Increasing the concentration of CO in the reducing gas increases the share of high-temperature electrolysis, improving the average electrolysis electrical efficiency. Increasing the carburization reduces the electricity demand of processing the DRI downstream in the EAF. The electricity demand of the process for a reducing gas CO concentration of 30% (by mole) and a degree of carburization of 1.5% (by weight) is 670 MW, a reduction of 17% compared to the H-DR case (806 MW). If only electricity would be used to pre-heat the reducing gas (i.e., no oxy-fuel combustion), as presented in Fig. 3, then the electricity demand of the H-DR case increases to 888 MW. The relative reduction in electricity demand achieved in the case with 30% (by mol) CO in the reducing gas and 1.5% (by weight) carburization is then 25%. This calculated electricity demand of the H-DR with purely electric pre-heating case agrees reasonably well with the results of Vogl et al. (2018): 3.48 MWh/t steel vs. 3.94 MWh/t steel here (assuming that all Fe in produced FeO remains in the final steel product and that all inert material in the pellets is separated out with the slag in the EAF). The higher estimate here is mainly due to a difference in assumed electrolyzer efficiency. For the case of 30% (by mole) CO in the reducing gas and a carburization of 1.5% (by weight), the specific electricity demand is 2.97 MWh/t steel.

The distribution of the total electricity consumption among the low-

and high-temperature electrolyzers, the EAF, and the reducing gas pre-heating in Fig. 11 is also of interest. It can be seen that the electrolyzers consume most of the electricity in all cases, with higher shares of high-temperature electrolysis at higher reducing gas CO concentrations. The EAF has the second highest electricity consumption, around 20% of the total. Increasing the degree of carburization with one percentage point is estimated to lower the overall electricity demand of the overall steelmaking process by roughly 3–4%. Electrical pre-heating of the reducing gas from 700 °C to 900 °C consumes a relatively small share of the total process electricity, around 5%.

The electricity demand of the steady state part of the process, i.e., the high-temperature electrolyzer, the EAF, and the electric pre-heating, increases with increasing reducing gas CO concentration; the result is that the minimum electricity demand of the process increases. The minimum electricity demand, excluding any CH₃OH production, increases from 215 MW in the case of H-DR to 539 MW in the case of 30% (by mole) of CO in the reducing gas and a DRI carburization of 1.5% (by weight). This increased minimum load may be disadvantageous during extended periods of high electricity prices, since this limits the dynamic operation of the process. However, it should be noted that the allowable low-temperature electrolyzer overcapacity also increases when increasing the reducing gas CO concentration, as seen in Fig. 7. Therefore, the total decrease in electricity demand flexibility of the process (here meaning the difference between the maximum and minimum electricity demand) when going from H-DR to 30% (by mole) CO and 1.5% (by weight) DRI carburization is only around 43% (from 866 MW to 493 MW of variability).

4.4. Total energy demand

The results of Fig. 10 and are combined in Fig. 12 (avoiding double counting of electric pre-heating). The overall energy demand of the process decreases with increasing reducing gas CO concentration, from a maximum of approximately 896 MW in the case of H-DR down to 823 MW for 1.5% (by weight) DRI carburization and 30% (by mole) of CO in the reducing gas.

Furthermore, as a larger share of the energy demand is made up of medium-temperature heat rather than electricity for cases with higher concentrations of CO in the reducing gas, the suggested process may be at an advantage over H-DR in terms of operational expenditure (OPEX),

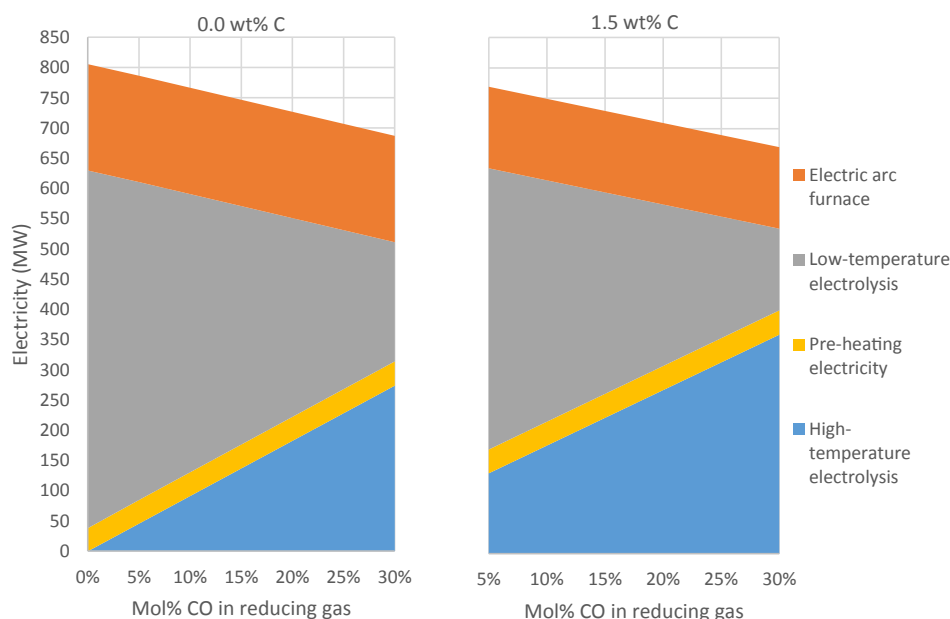


Fig. 11. Electricity demand of low- and high-temperature electrolyzers, the electric arc furnace, and reducing gas pre-heating for the supply of reducing gas as a function of reducing gas CO concentration for 0.0% (by weight) carburization (left) and 1.5% (by weight) carburization (right).

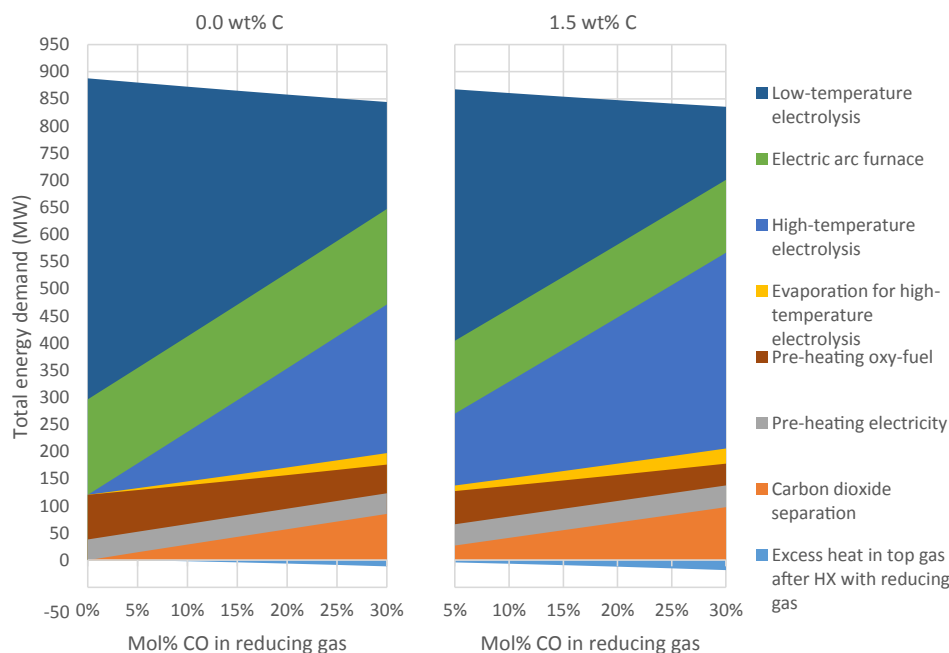


Fig. 12. Overall energy demand of suggested direct reduction process at full load as a function of reducing gas CO concentrations for 0.0% (by weight) DRI carburization (left) and 1.5% (by weight) DRI carburization (right).

especially in a case when the price of biomass is low relative to that of electricity. This may even be true for relatively low reducing gas CO concentrations and a low degree of DRI carburization.

5. Conclusion

A DR process incorporating a CH_3OH -based H_2 storage, high- and low-temperature electrolyzers, and oxy-fuel combustion of biomass was introduced and evaluated. The only inputs to this process are electricity, biomass, and iron ore pellets. Therefore, the net CO_2 emissions from the process should be significantly lower compared to the conventional BF-BOF steelmaking process under the condition that the consumed electricity is predominately generated from fossil-free sources.

The oxy-fuel combustion of biomass in combination with high-temperature co-electrolysis of CO_2 and H_2O allows for the introduction of CO into the reduction shaft, affecting the mass and energy balances of the overall process substantially. Most significantly, the electricity and total energy use of the process can be lowered by as much as 25% and 8% compared to the case of a pure H-DR process with electric pre-heating, respectively (17% reduction in electricity use if biomass oxy-fuel combustion is used for pre-heating in H-DR case). This decrease is mainly due to the higher efficiency of high-temperature electrolysis compared to low-temperature electrolysis and the introduction of biomass oxy-fuel combustion, which contributes significantly to the overall energy demand of the process. Secondly, the required supply of high-temperature heat is decreased when introducing CO into the process, although the demand for medium-temperature heat (at around 140 °C) increases significantly. A major share of this additional medium-temperature heat is used for the regeneration of the amine-based CO_2 absorption solution. However, despite this increase in the demand of medium-temperature heat, the overall energy demand of the DR process is found to decrease with increasing amounts of CO in the reducing gas, although the minimum electricity load of the process simultaneously increases, which may be a concern during extended periods of high electricity prices.

It is found that the integration of an oxy-fuel furnace and high-temperature electrolyzer allows for the storage of substantial amounts

of H_2 in the form of CH_3OH (from 181 up to 431 kt/y) using excess CO_2 in the process, i.e., there is no need for a dedicated supply of CO_2 for the production of CH_3OH , nor for a CO_2 storage. The maximum amount of CH_3OH that can be produced increases with increasing reducing gas CO content, and in the other end, the heat demand of the CH_3OH reformer is found to constitute a relatively small part of the overall heat demand of the process.

The results of this paper indicate that the suggested DR process is worth a more detailed evaluation. The process currently has many uncertainties and further research within a number of areas is required. Large-scale CH_3OH reforming with possible supply of O_2 , H_2O and CO_2 high-temperature co-electrolysis; oxy-fuel combustion of biomass; economic optimization of CH_3OH production capacity; and the performance of the process under dynamic conditions are particular areas that need further investigation.

CRediT authorship contribution statement

Joakim Andersson: Conceptualization, Methodology, Formal analysis, Software, Investigation, Visualization, Writing - original draft, Writing - review & editing. **Andries Krüger:** Formal analysis, Software, Investigation, Writing - original draft, Writing - review & editing. **Stefan Grönkvist:** Methodology, Formal analysis, Writing - review & editing, Project administration, Supervision, Funding acquisition.

Declaration of Competing Interest

The authors declare that they have no known competing financial interests or personal relationships that could have appeared to influence the work reported in this paper.

Acknowledgements

The work has been conducted as part of the HYBRIT research project RP-1. We gratefully acknowledge financial support from the Swedish Energy Agency.

References

- [1] Åhman, M., O. Olsson, V. Vogl, B. Nyqvist, A. Maltais, L.J. Nilsson, K. Hallding, K. Skåneberg, and M. Nilsson, Hydrogen steelmaking for a low-carbon economy: A joint LU-SEI working paper for the HYBRIT project. EESS report 109, 2018.
- [2] Birat, J.P., 16 - Carbon dioxide (CO₂) capture and storage technology in the iron and steel industry, in *Developments and Innovation in Carbon Dioxide (CO₂) Capture and Storage Technology*, M.M. Maroto-Valer, Editor. 2010, Woodhead Publishing. p. 492-521.
- [3] United Nations Framework Convention on Climate Change, Adoption of the Paris Agreement (FCCC/CP/2015/L. 9/Rev. 1). 2015.
- [4] Riksdagen, Överenskommelse om den svenska energipolitiken. 2016.
- [5] Ariyama T, Takahashi K, Kawashiri Y, Nouchi T. Diversification of the ironmaking process toward the long-term global goal for carbon dioxide mitigation. *J. Sustain. Metall.* 2019;1–19.
- [6] Gielen D, Saygin D, Taibi E, Birat JP. Renewables-based decarbonization and re-location of iron and steel making: a case study. *J Ind Ecol* 2020.
- [7] Vogl V, Åhman M, Nilsson LJ. Assessment of hydrogen direct reduction for fossil-free steelmaking. *J Cleaner Prod* 2018;203:736–45.
- [8] HYBRIT, Final, report HYBRIT – Hydrogen Breakthrough Ironmaking Technology 2018, Energimyndigheten.
- [9] Kruck, O., F. Crotogino, R. Prelicz, and T. Rudolph, Overview on all known underground storage technologies for hydrogen. HyUnder (2013 August) Deliverable, 2013(3.1).
- [10] Crotogino, F., Larger Scale Hydrogen Storage, in *Storing Energy*. 2016, Elsevier. p. 411–429.
- [11] Johansson, F., J. Spross, D. Damasceno, J. Johansson, and H. Stille, Investigation of research needs regarding the storage of hydrogen gas in lined rock caverns: Prestudy for Work Package 2.3 in HYBRIT Research Program 1. 2018, KTH Royal Institute of Technology.
- [12] Andersson J, Grönkvist S. Large-scale storage of hydrogen. *Int J Hydrogen Energy* 2019;44(23):11901–19.
- [13] Tsay Q, Ray W, Szekeley J. The modeling of hematite reduction with hydrogen plus carbon monoxide mixtures: Part II. The direct reduction process in a shaft furnace arrangement. *AIChE J* 1976;22(6):1072–9.
- [14] Parisi DR, Laborde MA. Modeling of counter current moving bed gas-solid reactor used in direct reduction of iron ore. *Chem Eng J* 2004;104(1–3):35–43.
- [15] Remus R, Monsonet MA, Roudier S, Sancho LD. Best available techniques (BAT) reference document for iron and steel production. Luxembourg: Publications Office of the European Union; 2013. p. 621.
- [16] Bender, M., T. Roussiere, H. Schelling, S. Schuster, and E. Schwab, Coupled Production of Steel and Chemicals. *Chemie Ingenieur Technik*.
- [17] Béchara R, Hamadeh H, Mirgaux O, Patisson F. Optimization of the iron ore direct reduction process through multiscale process modeling. *Materials* 2018;11(7):1094.
- [18] Zervas T, McMullan J, Williams B. Gas-based direct reduction processes for iron and steel production. *Int J Energy Res* 1996;20(2):157–85.
- [19] Anameric B, Kawatra SK. Properties and features of direct reduced iron. *Miner Process Extr Metall Rev* 2007;28(1):59–116.
- [20] Battle, T., U. Srivastava, J. Kopfle, R. Hunter, and J. McClelland, The direct reduction of iron, in *Treatise on Process Metallurgy: Industrial Processes*. 2014, Elsevier. p. 89-176.
- [21] Morris, A.E., Iron Resources and Direct Iron Production, in *Encyclopedia of Materials: Science and Technology*, K.H.J. Buschow, et al., Editors. 2001, Elsevier: Oxford. p. 4302-4310.
- [22] J.A. Lepinski, J.C.M., Gordon H. Geiger, Iron, in *Kirk-Othmer Encyclopedia of Chemical Technology*. 2005.
- [23] Kirschen M, Badr K, Pfeifer H. Influence of direct reduced iron on the energy balance of the electric arc furnace in steel industry. *Energy* 2011;36(10):6146–55.
- [24] Hornby S, Madias J, Torre F, ArcelorMittal A, Rosario S. Myths and realities of charging DRI/HBI in electric arc furnaces. *Iron Steel Technol*. 2016.
- [25] Memoli, F., Behavior and benefits of high-Fe3C DRI in the EAF. Vol. 2. 2015. 1928-1945.
- [26] Jess A, Depner H. Reduction and carburization of iron-ore in a fluidized bed by CO, H₂ and CH₄. *Steel Res.* 1998;69(3):77–84.
- [27] Cavaliere, P., Direct Reduced Iron: Most Efficient Technologies for Greenhouse Emissions Abatement, in *Clean Ironmaking and Steelmaking Processes*. 2019, Springer. p. 419-484.
- [28] Carpenter, A., CO₂ abatement in the iron and steel industry. IEA Clean Coal Centre, 2012: p. 67-70.
- [29] Kirschen M, Risonarta V, Pfeifer H. Energy efficiency and the influence of gas burners to the energy related carbon dioxide emissions of electric arc furnaces in steel industry. *Energy* 2009;34(9):1065–72.
- [30] Carpenter A. CO₂ abatement in the iron and steel industry. IEA Clean Coal Centre 2012:25.
- [31] Manocha S, Ponchon F. Management of Lime in Steel. *Metals* 2018;8(9):686.
- [32] Chatterjee A. Sponge iron production by direct reduction of iron oxide. PHI Learning Pvt. Ltd.; 2010.
- [33] Battle, T., U. Srivastava, J. Kopfle, R. Hunter, and J. McClelland, The direct reduction of iron, in *Treatise on process metallurgy*. 2014, Elsevier. p. 89-176.
- [34] Hamadeh H, Mirgaux O, Patisson F. Detailed modeling of the direct reduction of iron ore in a shaft furnace. *Materials* 2018;11(10):1865.
- [35] Xin Jiang Lin Wang Feng Man Shen Shaft Furnace Direct Reduction Technology - Midrex and Energiron AMR 805-806 654 659 10.4028/www.scientific.net/AMR.805-806 10.4028/www.scientific.net/AMR.805-806.654 https://www.scientific.net/AMR.805-806 https://www.scientific.net/AMR.805-806.654.
- [36] Duarte P, Becerra J, Lizcano C, Martinis A. Energiron Direct Reduction ironmaking-Economical, flexible, environmentally friendly. *Steel Times Int* 2010;34(3):25.
- [37] Bhaskar A, Assadi M, Somehsaraei N, Nikpey H. Decarbonization of the iron and steel industry with direct reduction of iron ore with green hydrogen. *Energies* 2020;13(3):758.
- [38] Fischedick M, Marzinkowski J, Winzer P, Weigel M. Techno-economic evaluation of innovative steel production technologies. *J Cleaner Prod* 2014;84:563–80.
- [39] Sasiain A, Rechberger K, Spanlang A, Kofler J, Wolfmeir H, Harris C, et al. Green hydrogen as decarbonization element for the steel industry. *BHM Berg-und Hüttenmännische Monatshefte* 2020:1–5.
- [40] Hölling, M. and S. Gellert, Direct Reduction: Transition from Natural Gas to Hydrogen? 2018.
- [41] Sundén, B. High temperature heat exchangers (HTHE). in *Proceedings of the 5th International Conference on Science, Engineering and Technology*, VIT University, Vellore, India. 2005.
- [42] Sheldon D. Methanol production-a technical history. *Johnson Matthey Technol Rev* 2017;61(3):172–82.
- [43] Goeppert A, Czaun M, Jones J-P, Prakash GS, Olah GA. Recycling of carbon dioxide to methanol and derived products-closing the loop. *Chem Soc Rev* 2014;43(23):7995–8048.
- [44] Andika R, Nandiyanto ABD, Putra ZA, Bilad MR, Kim Y, Yun CM, et al. Co-electrolysis for power-to-methanol applications. *Renew Sustain Energy Rev* 2018;95:227–41.
- [45] Álvarez A, Bansode A, Urakawa A, Bavykina AV, Wezendonk TA, Makkee M, et al. Challenges in the greener production of formates/formic acid, methanol, and DME by heterogeneously catalyzed CO₂ hydrogenation processes. *Chem Rev* 2017;117(14):9804–38.
- [46] Pontzen F, Liebner W, Gronemann V, Rothaemel M, Ahlers B. CO₂-based methanol and DME-Efficient technologies for industrial scale production. *Catal Today* 2011;171(1):242–50.
- [47] Perez-Forbes M, Schöneberger JC, Boulamanti A, Tzimas E. Methanol synthesis using captured CO₂ as raw material: techno-economic and environmental assessment. *Appl Energy* 2016;161:718–32.
- [48] Van-Dal ES, Bouallou C. Design and simulation of a methanol production plant from CO₂ hydrogenation. *J Cleaner Prod* 2013;57:38–45.
- [49] Marlin, D.S., E. Sarron, and Ó. Sigurbjörnsson, Process Advantages of Direct CO₂ to Methanol Synthesis. *Frontiers in chemistry*, 2018. 6.
- [50] Rihko-Struckmann LK, Peschel A, Hanke-Rauschenbach R, Sundmacher K. Assessment of methanol synthesis utilizing exhaust CO₂ for chemical storage of electrical energy. *Ind Eng Chem Res* 2010;49(21):11073–8.
- [51] Atonios K, Panopoulos KD, Kakaras E. Investigation of technical and economic aspects for methanol production through CO₂ hydrogenation. *Int J Hydrogen Energy* 2016;41(4):2202–14.
- [52] Bergins, C., K. Tran, E. Koitsoumpa, E. Kakaras, T. Buddenberg, and Ó. Sigurbjörnsson. Power to Methanol Solutions for Flexible and Sustainable Operations in Power and Process Industries. in *Power-Gen Europe*. 2015.
- [53] Nestler, F., M. Krüger, J. Full, M.J. Hadrich, R.J. White, and A. Schaadt, Methanol Synthesis-Industrial Challenges within a Changing Raw Material Landscape. *Chemie Ingenieur Technik*.
- [54] Ouda, M., C. Hank, F. Nestler, M. Hadrich, J. Full, A. Schaadt, and C. Hebling, Power-to-Methanol: Techno-Economical and Ecological Insights, in *Zukünftige Kraftstoffe*. 2019, Springer. p. 380-409.
- [55] Hank, C., S. Gelpke, A. Schnabl, R.J. White, J. Full, N. Wiebe, T. Smolinka, A. Schaadt, H.-M. Henning, C.J.S.E. Hebling, and Fuels, Economics & carbon dioxide avoidance cost of methanol production based on renewable hydrogen and recycled carbon dioxide-power-to-methanol. 2018. 2(6): p. 1244-1261.
- [56] Stieffel S, Berger A, Fernández Sanchis EM, Ziegmann M. Methodology for the evaluation of CO₂-based syntheses by coupling steel industry with chemical industry. *Chem Ing Tech* 2018.
- [57] Ruland H, Song H, Laudenschleger D, Stürmer S, Schmidt S, He J, et al. CO₂ hydrogenation with Cu/ZnO/Al₂O₃: a benchmark study. *ChemCatChem* 2020.
- [58] Zurbel A, Kraft M, Kavurucu-Schubert S, Bertau M. Methanol synthesis by CO₂ Hydrogenation over Cu/ZnO/Al₂O₃ catalysts under fluctuating conditions. *Chem Ing Tech* 2018;90(5):721–4.
- [59] Zhu Q. Developments on CO₂-utilization technologies. *Clean Energy* 2019;3(2):85–100.
- [60] Schweitzer, C. Small scale Methanol Plants: a chance for re-industrialisation. in *International Methanol Conference*. 2017. Copenhagen.
- [61] Lundgren J, Ekbohm T, Hultberg C, Larsson M, Grip C-E, Nilsson L, et al. Methanol production from steel-work off-gases and biomass based synthesis gas. *Appl Energy* 2013;112:431–9.
- [62] Hansson, J., R. Hackl, M. Taljegard, S. Brynolf, and M. Grahn, The Potential for Electrofuels Production in Sweden Utilizing Fossil and Biogenic CO₂ Point Sources. *Frontiers in Energy Research*, 2017. 5(4).
- [63] Toftegaard MB, Brix J, Jensen PA, Glarborg P, Jensen AD. Oxy-fuel combustion of solid fuels. *Prog Energy Combust Sci* 2010;36(5):581–625.
- [64] Nemitallah MA, Habib MA, Badr HM, Said SA, Jamal A, Ben-Mansour R, et al. Oxy-fuel combustion technology: current status, applications, and trends. *Int J Energy Res* 2017;41(12):1670–708.
- [65] Lüke L, Zschocke A. Alkaline water electrolysis: efficient bridge to CO₂-emission-free economy. *Chem Ing Tech* 2020;92(1–2):70–3.
- [66] Buttler A, Spliethoff H. Current status of water electrolysis for energy storage, grid balancing and sector coupling via power-to-gas and power-to-liquids: a review. *Renew Sustain Energy Rev* 2018;82:2440–54.
- [67] Schmidt O, Gambhir A, Staffell I, Hawkes A, Nelson J, Few S. Future cost and performance of water electrolysis: an expert elicitation study. *Int J Hydrogen*

- Energy 2017;42(52):30470–92.
- [68] Ni M, Leung MK, Leung DY. Technological development of hydrogen production by solid oxide electrolyzer cell (SOEC). *Int J Hydrogen Energy* 2008;33(9):2337–54.
- [69] Bhandari R, Trudewind CA, Zapp P. Life cycle assessment of hydrogen production via electrolysis—a review. *J Cleaner Prod* 2014;85:151–63.
- [70] Sun X, Chen M, Jensen SH, Ebbesen SD, Graves C, Mogensen M. Thermodynamic analysis of synthetic hydrocarbon fuel production in pressurized solid oxide electrolysis cells. *Int J Hydrogen Energy* 2012;37(22):17101–10.
- [71] Samavati M, Santarelli M, Martin A, Nemanova V. Thermodynamic and economy analysis of solid oxide electrolyser system for syngas production. *Energy* 2017;122:37–49.
- [72] Behrens, M. and M. Armbrüster, Methanol Steam Reforming, in *Catalysis for Alternative Energy Generation*, L. Guzzi and A. Erdöhelyi, Editors. 2012, Springer New York: New York, NY. p. 175–235.
- [73] Geissler K, Newson E, Vogel F, Truong T-B, Hottinger P, Wokaun A. Autothermal methanol reforming for hydrogen production in fuel cell applications. *PCCP* 2001;3(3):289–93.
- [74] Lattner JR, Harold MP. Autothermal reforming of methanol: experiments and modeling. *Catal Today* 2007;120(1):78–89.
- [75] Choi Y, Stenger H. Kinetics of methanol decomposition and water gas shift reaction on a commercial Cu-ZnO/Al₂O₃ catalyst. *Prepr. Pap.-Am. Chem. Soc., Div. Fuel Chem* 2002;47(2):723–4.
- [76] Edwards N, Ellis SR, Frost JC, Golunski SE, van Keulen ANJ, Lindewald NG, et al. On-board hydrogen generation for transport applications: the HotSpot™ methanol processor. *J Power Sources* 1998;71(1):123–8.
- [77] Wang M, Lawal A, Stephenson P, Sidders J, Ramshaw C. Post-combustion CO₂ capture with chemical absorption: a state-of-the-art review. *Chem Eng Res Des* 2011;89(9):1609–24.
- [78] Kopfle, J.T. and G.E. Metius. Environmental benefits of natural gas direct reduction. in *American Iron and Steel Society*, editor. AISTech 2010 conference proceedings. Pittsburgh: American Iron and Steel Society. 2010.
- [79] Rochelle GT. Amine scrubbing for CO₂ capture. *Science* 2009;325(5948):1652–4.
- [80] Onoda M, Matsuzaki Y, Chowdhury FA, Yamada H, Goto K, Tonomura S. Sustainable aspects of ultimate reduction of CO₂ in the steelmaking process (COURSE50 Project), part 2: CO₂ capture. *J. Sustain. Metal*. 2016;2(3):209–15.
- [81] Bui M, Adjiman CS, Bardow A, Anthony EJ, Boston A, Brown S, et al. Carbon capture and storage (CCS): the way forward. *Energy Environ Sci* 2018;11(5):1062–176.
- [82] NIST, N., Standard Reference Database 69: NIST Chemistry WebBook. National Institute of Standards and Technology, 2010.
- [83] Liu B, Li Q, Zou Z, Yu A. Discussion on chemical energy utilisation of reducing gas in reduction shaft furnace. *Ironmaking Steelmaking* 2014;41(8):568–74.
- [84] Yi L-Y, Huang Z-C, Peng H, Jiang T. Action rules of H₂ and CO in gas-based direct reduction of iron ore pellets. *J. Central South Univ.* 2012;19(8):2291–6.
- [85] Duarte P. Trends in hydrogen steelmaking. *Steel Times International* 2020;44(1):35–9.
- [86] Wester L. Tabeller och diagram för energitekniska beräkningar 1996.
- [87] Rao AB, Rubin ES, Berkenpas MB. An integrated modeling framework for carbon management technologies. *Carnegie Mellon University (US)*; 2004.
- [88] Ramezan, M., T.J. Skone, N. Nsakala, G. Liljedahl, L. Gearhart, R. Hestermann, and B. Rederstorff, Carbon dioxide capture from existing coal-fired power plants. *National Energy Technology Laboratory, DOE/NETL Report*, 2007. 401: p. 110907.
- [89] Bertuccioli, L., A. Chan, D. Hart, F. Lehner, B. Madden, and E. Standen, Development of water electrolysis in the European Union. *Fuel cells and hydrogen joint undertaking*, 2014. 83.
- [90] Kaur G, Kulkarni AP, Giddey S, Badwal SP. Ceramic composite cathodes for CO₂ conversion to CO in solid oxide electrolysis cells. *Appl Energy* 2018;221:131–8.
- [91] Zhang W, Yu B, Wang X, Chen J. Thermodynamic analysis of the efficiency of high temperature co-electrolysis system for syngas production. *Int J Hydrogen Energy* 2016;41(36):15960–9.
- [92] Stempien JP, Ding OL, Sun Q, Chan SH. Energy and exergy analysis of Solid Oxide Electrolyser Cell (SOEC) working as a CO₂ mitigation device. *Int J Hydrogen Energy* 2012;37(19):14518–27.
- [93] Peterson, D. and E. Miller, Hydrogen Production Cost from Solid Oxide Electrolysis. *Department of Energy-USA*, 2016.
- [94] Kazempoor P, Braun R. Hydrogen and synthetic fuel production using high temperature solid oxide electrolysis cells (SOECs). *Int J Hydrogen Energy* 2015;40(9):3599–612.
- [95] Hakkila, P., M. Parikka, Fuel resources from the forest, in *Bioenergy from sustainable forestry*. 2002, Springer. p. 19–48.
- [96] Iulianelli A, Ribeirinha P, Mendes A, Basile A. Methanol steam reforming for hydrogen generation via conventional and membrane reactors: a review. *Renew Sustain Energy Rev* 2014;29:355–68.
- [97] Zugliano A, Primavera A, Pignatone D, Martinis A. Online modelling of energiron direct reduction shaft furnaces. *IFAC Proceedings Volumes* 2013;46(16):346–51.
- [98] Rao, Y. and P. Pichestapong. Modelling of the Midrex direct-reduction ironmaking process: mass transfer and virtual equilibrium at steady state. in *XVth CMMI Congress. Metals Technology and Extractive Metallurgy*. 1994.
- [99] Bergins, C., T. Buddenberg, E.-I. Koytsoumpa, M.J. Duarte, E. Kakaras, S. Schmidt, and A. Deierling, A Technology Review and Cost Analysis of the Production of Low Carbon Methanol and Following Methanol to Gasoline Process, in *Zukünftige Kraftstoffe*. 2019, Springer. p. 433–463.